

JUNE 2002
VOL. 12, NO. 2



SPIE's
International
Technical
Group
Newsletter

ELECTRONIC IMAGING

Automatic digital restoration of faded color films

Calendar — See page 10

**Technical Group Registration
Form** — See page 11

NEWSLETTER NOW AVAILABLE ON-LINE

Technical Group members are being offered the option of receiving the Electronic Imaging Newsletter electronically. An e-mail is being sent to all group members with advice of the web location for this issue, and asking members to choose between the electronic and printed version for future issues. If you are a member and have not yet received this message, then SPIE does not have your correct e-mail address.

To receive future issues electronically please send your e-mail address to:

spie-membership@spie.org
with the word **EI** in the subject line of the message and the words **electronic version** in the body of the message.

If you prefer to receive the newsletter in the printed format, but want to send your correct e-mail address for our database, include the words **print version preferred** in the body of your message.

Motion pictures represent an important part of our collective memory. Since the 1950s, *monopack* color film became the standard upon which millions of cinematographic works were recorded. A couple of decades later, it turned out that this process was unstable, causing the fading of entire film stocks with time. The fading of one or two chromatic layers of the film results in a drab image with poor saturation and an overall color cast (see Figure 1(a)). Usually, a bleached, color-release print is the only available record of a film. Since the bleaching phenomenon is irreversible, photochemical restoration of faded prints is not possible: hence the necessity for digital color restoration.

A typical digital film restoration system,¹ illustrated in Figure 2, digitizes a film, processes it, then puts the images back on the film. This system can be used for all post-production processes (including special effects) but it is crucial that the whole system be chromatically calibrated to ensure reliable measurements. Our automatic technique² for faded film restoration, on the other hand, revives

the drab colors through an original saturation-enhancement technique. After this, the colors are balanced by an original method inspired by color-constancy algorithms.

Saturation-enhancement techniques usually work by uniformly increasing the saturation all over the image. They operate on a color space with a separate saturation channel like *HSV* or *L*C*h**, and the saturation increase is achieved by multiplying the saturation channel by a coefficient. These techniques are simple and give good results for intact images, but they are not suitable for faded images as they strengthen the color cast, yielding an image that is even more complex to restore.

Our color-enhancement technique is based on principal-component analysis (PCA) of the image in *L*a*b** space. It consists of scaling up, by a multiplicative factor, the *Lab* cloud according to the principal axes. Since these axes give the directions in which the *L*a*b** point set is stretched most, zones at the extremes of these axes show

Continued on page 8.



(a)



(b)

Figure 1. (a) Original faded image. (b) Image after restoration.

Edge detection via a fuzzy switch

Edge detection is the first step for some boundary-extraction and representation algorithms, and has been playing an important role in solving image-recognition and data-retrieval problems. For example, in the processing of cancer-cell images, once the edges of the cancer cells are detected, the shapes of the cancer cells can be seen more clearly. As the shapes of the cancer cells provide useful information for the medical professionals to decide their type, the technique helps to reduce the time for—and improves the accuracy of—the diagnosis procedure.

Some traditional methods—such as the Sobel, Prewitt, Roberts, Isotropic and Canny filters—have been considered. These are based on convolving an image with the impulse-response of a linear, spatially-invariant filter that approximates either the first- or second-order derivatives. However, when the image suffers from noise, there is a trade-off between the detection error (signal-to-noise ratio) and the localization (the reciprocal of the root-mean-squared distance of the marked edge from the center of the true edge). The optimal filter is the derivative of a Gaussian filter.

To work on this problem, a combination of conditioning, feature extraction, blending and scaling has been proposed.¹ Conditioning enhances the raw sensor data for further processing, some examples of which include contrast enhancement and histogram equalization. Feature extraction pulls out feature vectors that contain edge information. The most common are Sobel, Prewitt, and range and standard deviation features. Blending involves the aggregation of components of feature vectors. The inner product or Minkowski norms, generalized logistic functions (such as waterfall functions), and computational learning models (such as neural-like network models and Takagi-Sugeno fuzzy reasoning models), have been used so far.¹ Finally, scaling allows gray levels or crisp points to be taken from raw edge images. Dynamic scaling was used in the previously mentioned work.

However, different feature vectors have different properties at the edge points. For example, Sobel features approximate a first-order derivative, and so give a maximum value at an edge point. On the other hand, Laplace features approximate a second-order derivative: zero at an edge point. We should consider these properties when designing blending functions to aggregate different components of the feature vectors together. This is also important because, if a blending function gives a weighted sum of each element in the feature vectors, then the edge will be blurred because a lowpass effect will be introduced at the output.

Instead, we model an edge detector as a fuzzy switch (shown in Figure 1). Here, the expert systems are the edge detectors, which capture the knowledge from different experts, and their out-

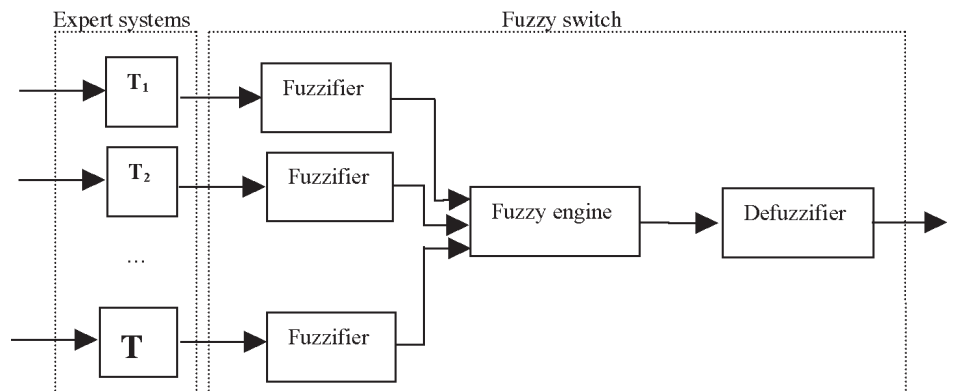


Figure 1. Fuzzy edge detector.

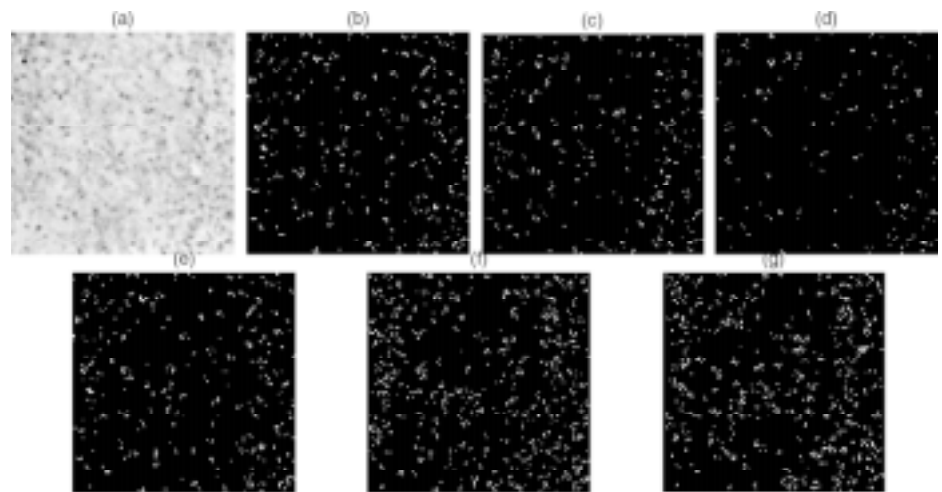


Figure 2. Results of different edge detectors on the image 'Cancer': (a) original image; (b) output of Sobel filter; (c) output of Prewitt filter; (d) output of Roberts filter; (e) output of Isotropic filter; (f) output of Canny filter; and (g) output of our proposed fuzzy switch.

puts form a feature vector providing useful edge information. The fuzzifiers are used to normalize the values of the elements in the feature vector. The fuzzy engine (fuzzy switch) is used to aggregate the feature-vector components. Finally, the defuzzifier maps the output of the fuzzy engine to a crisp point that represents an edge point.

For the expert systems, we selected common gradient and compass operators, such as the Sobel, Prewitt, Roberts, Isotropic, Canny and Kirsch filters. For the blending function, we selected the maximum value of the feature vector.

Results

We tested a 512×512 image, *Cancer*, using some of the well-known gradient operators described above and our proposed algorithm. The simulation results show that the Canny edge detector produces too many details, that the skeletons of

the images are lost, and that the output is noisy in some regions. On the other hand, the Prewitt and Roberts filters produce too little information at the outputs, so the edges are mainly discontinuous. In comparison, our proposed algorithm captures the advantages of the different expert systems, so producing the best results.

Wing-kuen Ling and Kwong-Shun Tam
 Room CD514, Department of Electronic and Information Engineering
 The Hong Kong Polytechnic University
 Hung Hom, Kowloon, Hong Kong, China
 E-mail: bingob@eie.polyu.edu.hk

References

1. J. C. Bezdek, R. Chandraskhar and Y. Attikiouzel, *A Geometric Approach to Edge Detection*, **IEEE Transactions on Fuzzy Systems** 6 (1), pp. 52-75, February 1998.

Natural vision: spectrum-based natural-color image reproduction system

In the color imaging systems used for electronic commerce, tele-medicine, digital museums, and educational material, the realism of the reproduced image is very important. The colors reproduced by current imaging systems are, however, device dependent, illumination dependent, and/or observer dependent, and so, for instance, we observe somewhat different color images on television or computer displays.

Akasaka Natural Vision Research Center (NVRC) was established by Telecommunication Advancement Organization (TAO) under the support of the Ministry of Public Management, Home Affairs, Post and Telecommunication (MPHPT) Japan, for the purpose of developing a visual communication system with natural color, overcoming the limitation of current RGB-based systems. The project started 1999 and has just been extended. Participants include Tokyo Institute of Technology, Chiba University, NTT, NTT Data, Olympus Optical, Matsushita Electric, Hitachi, NHK, Toppan Printing, and Dai Nippon Printing. The prototype natural vision system includes multi-spectral cameras (MSC—16-band still image and six-band HDTV), and six-primary-color projection displays (2x2-tiled LCD projectors, see Figure 1, and DLP projectors). Our results so far¹ are presented here.

Multi-spectral imaging allows us to acquire the spectral radiance or reflectance, resulting in a great improvement in colorimetric accuracy under the illumination of arbitrary spectra. Multi-primary-color display, i.e., using more than three primary colors, allows the reproduction of a wider color gamut, as well as spectral color reproduction. Both are thus important technologies for high-fidelity color reproduction.

Conventional color management systems are based on three-dimensional color space, and it is therefore impossible to implement illumination conversion and spectral color reproduction. For the management of multi-spectral and multi-primary image data, we use the spectrum-based color reproduction system shown in Figure 2. The image data is accompanied by details of the conditions under which the image was captured (source profile): i.e. spectral sensitivity of the camera, illumination spectrum, etc. The architecture is similar to the ICC (International Color Consortium)



Figure 1. Our 2x2-tiled six-primary LCD projection display system.

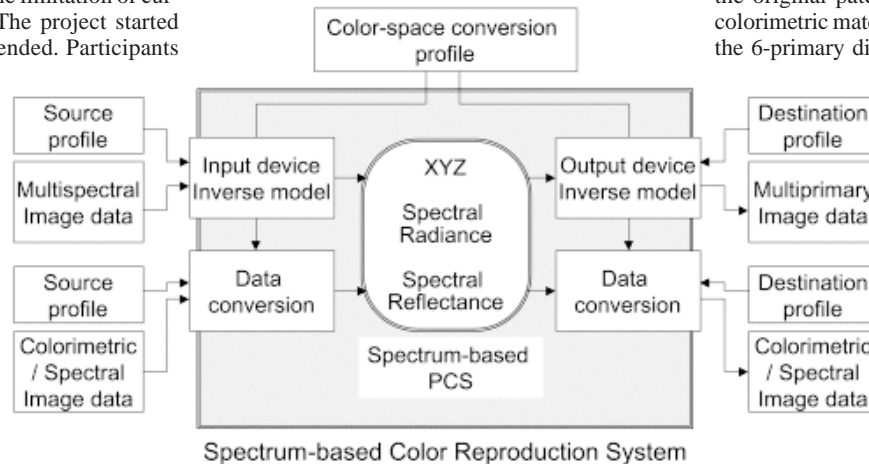


Figure 2. Schematic diagram of the spectrum-based color reproduction system.

color management system, but the profile connection space (PCS) is not based on the color-appearance model, but the physical model, i.e. the spectrum-based PCS (SPCS). This can be any CIEXYZ under arbitrary illumination, spectral radiance, or spectral reflectance.

Our system realizes: color reproduction using arbitrary color imaging devices that have three-or-more channels under the illumination of an arbitrary spectrum; spectral reflectance reproduction; and color reproduction based on unconventional color-matching functions (CMFs) to discount CMF variation among observers. Using the source profile attached to the image, moreover, the multi-spectral image data can be used for spectral image analysis: useful for object recognition, spectral feature extraction, and spectral measurement.

We have experimentally evaluated the colorimetric reproduction accuracies of the 16-band MSC and six-primary display, and average and

maximum DE^*ab of both camera and display are about 1.0 and 2.0, respectively. Wider color gamut is also obtained by the six-primary display as previously reported.²

We have also demonstrated that the influence of CMF variation among observers becomes negligible using the multi-primary display. The actual color patches are visually compared with the reproduced colors by RGB-based and six-primary-based displays. The display signals for six channels are calculated such that the spectral difference between the original and reproduced colors are minimized where the colorimetric match is kept. Through tests with eight observers tests, the colors reproduced by RGB-based displays sometimes look different from the original patch, although all colors satisfy colorimetric match, and the color reproduced by the 6-primary display is the best match for all observers. This means the color matching between printed and display media is improved by reducing the spectral difference between printed and reproduced colors.

The spectrum-based color reproduction system presented in this paper can handle any type of imaging media, including cameras, scanners, and displays with three-or-more channels, and high-fidelity color reproduction becomes possible based on the physical model. Psychophysical models, such as color-appearance models, preferable color reproduction, and computer graphics, can be also employed in conjunction with the presented spectrum-based color reproduction system.

Masahiro Yamaguchi

Tokyo Institute of Technology
Imaging Science & Engineering Laboratory
4259 Nagatsuta, Midori-ku
Yokohama 227-8503, Japan
E-mail: guchi@isl.titech.ac.jp

References

1. M. Yamaguchi, T. Teraji, K. Ohsawa, T. Uchiyama, H. Motomura, Y. Murakami, and N. Ohshima, *Color image reproduction based on the multispectral and multiprimary imaging: Experimental evaluation*, **Proc. SPIE 4663**, pp.15-26, 2002.
2. T. Ajito, T. Obi, M. Yamaguchi, and N. Ohshima, *Expanded color gamut reproduced by the six-primary projection display*, **Proc. SPIE 3954**, pp.130-137, 2000.

Median in spatial and frequency domain filtering

“Give me a lever long enough, and a prop strong enough, and I can singlehandedly move the world.”

—Archimedes

We would like to discuss the development of the notion of the median, which is widely used for impulsive-noise filtering. This notion introduces an important criterion for impulse detection in its local window (we will call the image values taken from the filtering window and sorted in ascending order as a *variational set*). Normally, the removal of impulses in an image by replacing their value by the median would be considered a very bad idea, because it is a destructive measure. But the median filter is based on the idea that the impulse will always lie on one of the ends of the variational set. This gives an excellent criterion for impulse detection, which can be done *a priori* to any filtering. To be more specific, the only thing needed is to check the observed pixel value, to see if it lies close to one of the ends of variational set taken from the pixel's local window. The closer it is to one of the ends, the higher the chance that it contains an impulse that has to be eliminated. Depending on the distance, a different number of pixels will be filtered: but this is still much better than filtering of *all* the pixels. This simple impulse detector can be used not just in impulse noise filters, but also other filters so that impulses will not affect the result. The simplest example of such filter is probably the *a*-trimmed mean filter.

Back to the main subject: a few interesting points have been raised. The first is the detection of the impulses in spatial domain, performed by checking the distance from the ends of the variational set. However, if we look at it from the opposite point of view, this is the same as checking the distance from the median. It turns out that by applying an exponential function to the difference between the observed pixel value and the median leads to even stronger impulse detection. This method can effectively detect impulsive noise on the image with a corruption rate of 10% (see Figure 1). Here, we compare the



Figure 1. Impulsive noise filtering using a preliminary exponential noise detector. (a) The input image is corrupted by impulsive noise (15% corruption rate); (b) the result of filtering using the exponential noise detector; (c) the result of filtering using the simple median filter.

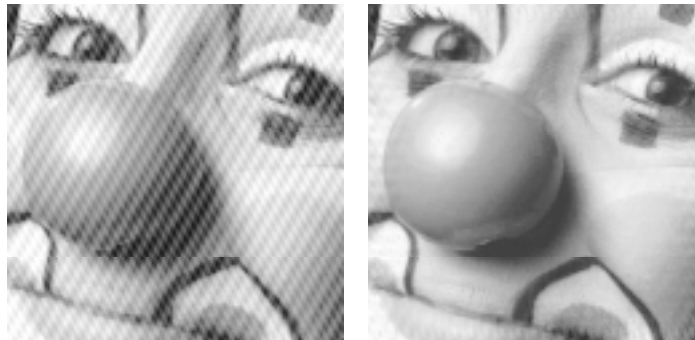


Figure 2. Quasi-periodic noise removal using the median detector and Gaussian surface filtering in the frequency domain. (a) The input noisy image. (b) The filtering result.

exponent of difference to some threshold: if it's higher we say that pixel is corrupted. The steepness of the exponent can be modified to adjust the sensitivity to threshold.

Now let us jump to the frequency domain or, more precisely, the Fourier spectrum's amplitude domain. It is well known that periodic and quasi-periodic noise is represented by peaks in the Fourier spectrum. This suggests the idea of using the median for removal of these peaks. Here, the coefficient of interest is not checked for its distance from the ends of variational set (which is built of spectral coefficients around the analyzed coefficient), nor for distance from the median. Instead, the ratio of the coefficient-of-interest to the median is calculated. This ratio is compared to the threshold and, if it's larger than the coefficient, it is considered to be a peak and eliminated. This is the idea behind the spectral peak detector.

From here, ideas for two peak eliminators are suggested. The first involves the replacement of the spectral coefficient by the median, just as in the usual median filter, flattening the peak

and the whole surface around it. The second approach requires more explanation. The periodic distortions in the spectrum rarely take the form of a single impulse: they usually look like a steep hill. Using the median to replace the peak will smooth this hill somewhat, but not eliminate it. These hills look very similar to a

two-dimensional Gaussian surface, which suggests the idea of taking this surface (its values must vary from 0 to 1), inverting it by subtracting it from 1 and multiplying the spectral hill by this surface. This way the hill will be completely removed and, a possible drawback of this method, the peak will be set to 0. Of course, a scaling coefficient can be introduced so the peak will not be set to 0 but just reduced by some amount. Also, the steepness of the Gaussian surface can be modified to better filter noise.

Consequently, these approaches work well for different scenarios: median is good when the periodic structure introduces singular peaks, or peaks with a few smaller peaks around it. The surface method is best when the periodic structure introduces wide hills (see Figure 2). Of course, it should be noted that the surface could be compressed such that it will just replace the peak (one coefficient) with 0 and leave the vicinity intact. But, for this scenario, the median technique is preferred. The third and final modification to the surface technique is to adapt it to each filtering window such that, after filtering the peak, it will become equal to the median instead of 0. This necessitates the scaling of the surface.

Igor Aizenberg and Constantine Butakoff
Mapu 18, Ap.3, Tel Aviv, 63434 Israel
E-mail: igora@netvision.net.il,
cbutakoff@ukr.net
<http://vega.0catch.com>

Electronic imaging for the inspection of wooden planks

The need for automatic visual inspection is becoming critical in the wood industry in order to maintain and improve productivity and quality. In practice, a system capable of sensing, recognizing, and measuring the sizes and relative positions of individual defects—and, finally, classifying the piece of wood—is required. The major problems in grading wood boards usually come down to the very high rate of production, the large number of defect classes and the high inherent variability. On a typical line, boards travel at speeds of $0.5\text{--}2\text{ms}^{-1}$. The main standards of the major European countries list over 400 different quality classes. Also, no two boards or defects have exactly the same properties of color and texture. Here, we show a methodology for wood defect detection and classification achieved through two parallel operations: detection of biological (knots, checks, resin pockets, stain, pitch, etc) and mechanical (width, thickness, curvatures, split and cracks) defects. A combination of two cameras and one laser-line generator performs this task for each side of the plank, as is shown in Figure 1.

Camera #1 acquires a grey-level image $s(i,j)$ detecting the biological defects while Camera #2 ($f(i,j)$) searches for mechanical deformations. An appropriate grey-level threshold, used for image-segmentation into wood and background (Figure 2(b)), is calculated automatically by performing a histogram analysis. The binary image obtained may be noisy, as is shown in Figure 2(b) and (c), so the basic assumption is that all data in the binary image that do *not* represent defects or background are due to noise.

To filter this out from the binary image, two filtering steps are implemented: morphological filtering, and averaging. These result in a reduced binary image, and possible defects are isolated as non-connected binary objects inside it, as is shown in Figure 2(d).

The sequential component-labelling algorithm identifies each non-connected component. The objects labelled as 1 and 2 represent the first and second defects. The recursive labelling algorithm requires large memory stack, which can produce problems when labelling samples with a large concentration of defects. During the connected-components analysis of the image, the shape features for the blobs being investigated can be collected and stored: these include defect dimension, area, number of thresholded pixels, and moment as well as features derived from these, such as lengths of principal axes, aspect

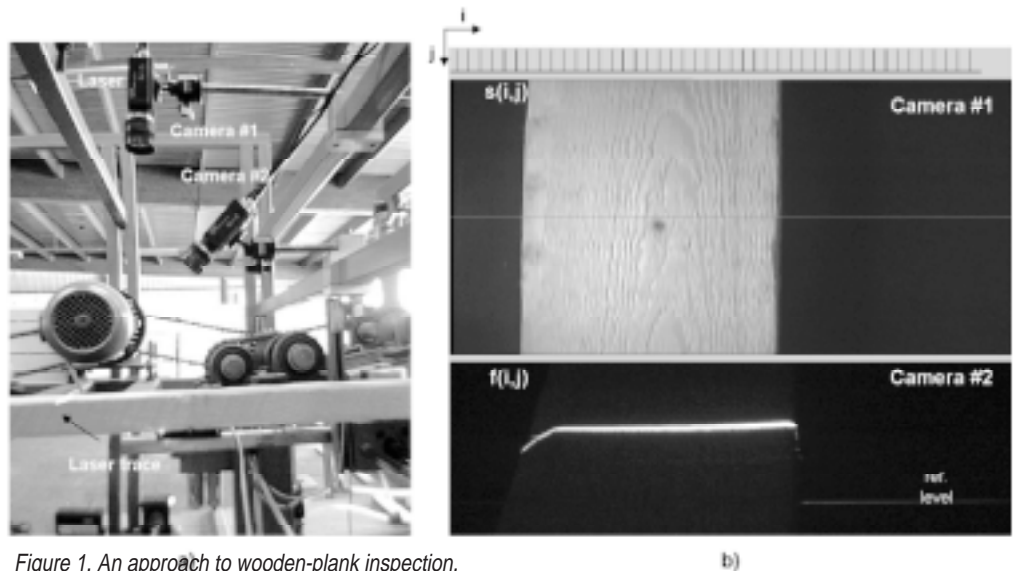


Figure 1. An approach to wooden-plank inspection.

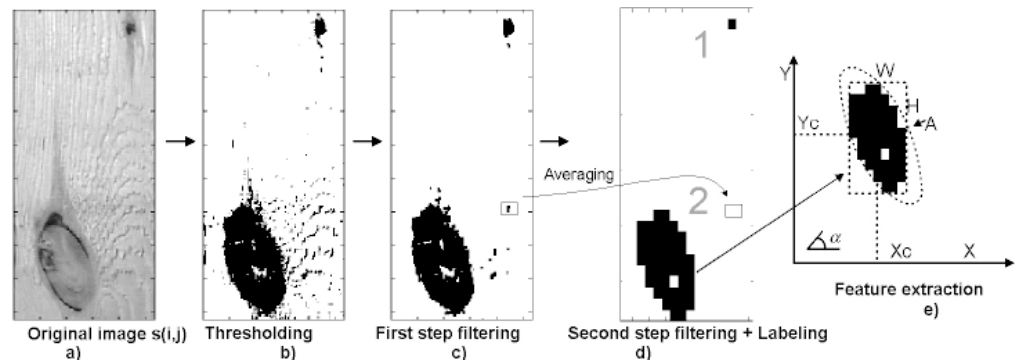


Figure 2. Detection of biological defects: algorithmic steps.

ratio, angle, etc. Moment-based features are useful in determining the defect dimensions. The angle parameter is less important in knot analysis because the knot can be oriented in practically any angle. It is a very important parameter in the detection of split orientation, on the other hand. To increase the overall processing speed, the following five features suffice: length of defect (H), width of defect (W), position (X_c, Y_c), aspect ratio of ellipse fitted ($R=\text{major_axe}/\text{minor_axe}$) and compactness, i.e. filled ratio, ($C=H*W/A$, $A=\text{area}$). See Figure 2(e).

Mechanical defects are detected by analysing the laser trace inside the image $f(i,j)$, produced by optical triangulation using camera #2 and the laser line. To obtain better trace distinction from the background, and to minimize useless light variations and noise, an optical band-pass interference filter (670nm) is mounted in front of the camera lens. Our objective is not the whole image $f(i,j)$, but only the vector $Y(i)$, which represents the laser trace

(Figure 3(a)). Grouping the vectors $Y(i)$ taken over time t generates a 3D surface of the wood (see Figure 3(a)). From $Y(i)$ we extract different features such as the thickness in different points, the width in different levels and the number of cracks or splits. Analyzing the plank profile at a minimum of three horizontal and three vertical positions is sufficient for a rough geometric estimation: the profile of a plank sample does not change drastically. Splits and cracks can be seen as impulses in the profile vector, as is shown in Figure 3(b). To emphasize these peaks, different techniques, such as Windowed Standard Deviation (WSD) and Windowed Contrast in Horizontal Direction (WCHD), can be employed as is shown. After filtering out the cracks, the automated thresholding is implemented. The resulting binary vector gives the number of detected cracks by counting the groups of separated strings of

Continues on page 9.

Shape representation for color image querying

Recent advances in internet technology demand a better methodology for accessing world wide web (www) sites and supporting image databases. Indexing the content of web pages and frames for query and retrieval will be a the key operation for enhanced media usage. A variety of approaches have been developed to deal with the visual-content search-and-retrieval issue in web-based applications.¹⁻⁵ The majority of these approaches select either shape² or color^{3,4} information, or combination of both,⁶ as the key features or indices in their search process. Since the use of spectral and spatial information is expected to yield a consistent search result, there is a need for a systematic way of integrating these two sources of information for a given image or a web page. This integration is essential in many multimedia information-processing and transmission systems involving addressable picture and video databases, especially for such applications as trademark logos, facial identification, fingerprint analysis, digital library databases, collaborative video teleconferencing, and virtual navigation.

For this purpose, we adopt the Radon transform⁷ for packing the shape information. Our earlier research work⁸ has demonstrated that the Radon transform is effective for converting the two-dimensional (2D) figure to a one-dimensional (1D) signal representation. In this transformation, a flat object of intensity $f(x,y)$ is integrated along the s -axis, which results in a 2D-to-1D transformation denoted by $g(s, \theta)$ as shown in Figure 1. The function $g(s, \theta)$ is the 1D projection of $f(x,y)$ at offset s and at an angle θ . A translation of $f(x,y)$ results in the shift of $g(s, \theta)$ in s and a rotation of the object causes a translation of $g(s, \theta)$ in θ . This transformation is applied to each color channel separately for projection angles varying between 1° and 180° in 1° intervals. The shortest and longest Radon transforms are selected as the most distinctive attributes of the object shape being queried. For the inclusion of spectral features in context indexing, we employ the Kullback-Leibler distance (KLD)⁹ histogram-comparison method to compute the similarity between the corresponding Radon transforms of the query and database images. KLD is the asymptotic limit of the maximum likelihood criterion, and

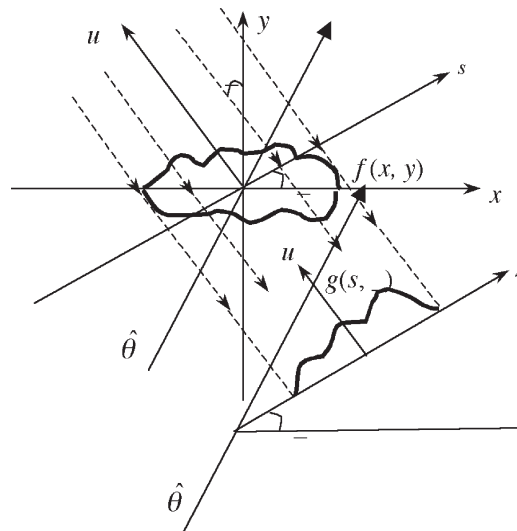


Figure 1. 1D projection $g(s, \theta)$ of 2D function $f(x,y)$ at angle θ .

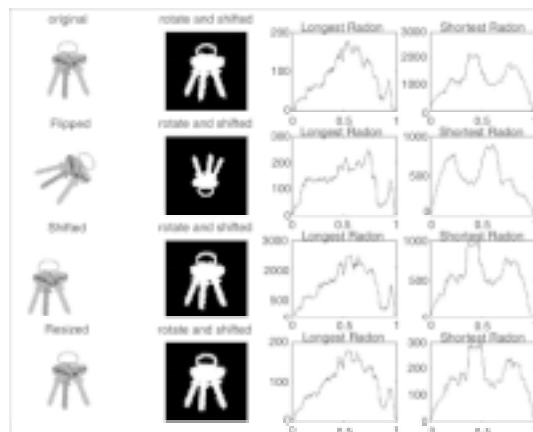


Figure 2. Greyscale images of keys representing the implementation details.

Table 1. Similarity measure for sets of images considered in Figure 3.

	Pic#1	Pic#2	Pic#3	Pic#4	Pic#5	Pic#6	Pic#7	Pic#8
Pic#1	0	97.1	164.9	181.4	103.7	138.7	83.3	133.6
Pic#2	97.1	0	145.6	175.1	175.6	210.5	197.6	203.8
Pic#3	165	145.6	0	12.3	148	138	161.2	150.9
Pic#4	181.4	175.1	12.3	0	159.9	161	184.5	177.1
Pic#5	103.7	175.6	148	160	0	30	62.5	60
Pic#6	128.7	210.5	138	161	30	0	78.3	49.3
Pic#7	83.3	197.6	161.2	184.5	62.5	78.3	0	38.3
Pic#8	133.6	203.8	150.9	177.1	60	49.3	38.3	0

thereby a good method for comparing distributions. In this case, it is performed on each color channel separately and the results are summed together to form a similarity measure.

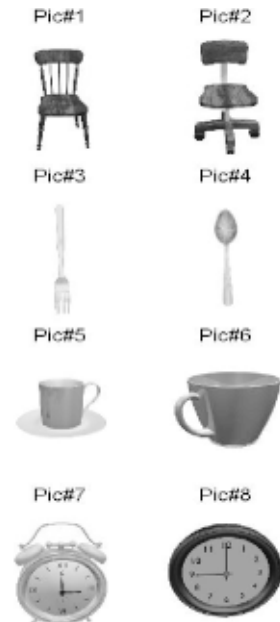


Figure 3. Distinctive shape classes used for testing the efficacy of the method.

In the current approach, a high-quality, uncompressed color picture is used as the query input. Using the Hotelling (discrete Karhunen-Loeve) transform,¹⁰ the image origin is translated to the object center, and then the coordinate axes aligned with the major and minor principal lines of elongation of the object shape. This method is effective for translation- and rotation-invariant retrieval. Size invariance is achieved by normalizing the object bounding-box,¹¹ in which shape and color content are sought.

The proposed algorithm was implemented in Matlab-6, using a wide range of objects imaged in 24bits per color with different spatial resolutions. Implementation details are illustrated using a set of binary pictures of a key bunch in different positions and sizes as shown in Figure 2. The KLDs between two images are calculated in the longest and shortest directions of the Radon transform, and then are added together to find the similarity measure between the query and database pictures. Higher measurement values indicate dissimilar shapes while the smaller results represent similar ones. For the objects in Figure 2, we computed the similarity measure between the original and reconstructed (i.e., flipped, shifted, and resized) shapes as 28.9, 16.4, and 11.7; between the flipped and shifted as 19.7; and the flipped and resized as 17, respectively. For the shifted and resized shapes, we obtained a distance of 6.4. From these

Continues on page 8.

Automatic surface inspection of raw milled-steel blocks using range imaging

In the steel industry there is an increasing demand for automatic inspection systems to control the quality of products. Image processing techniques will therefore play a crucial role in this growing field. Demanding customer requirements are well-founded given the high costs of fixing a poor quality product. In the literature, two different approaches for acquiring surface images are generally considered: intensity imaging techniques, e.g. diffuse illumination, bright-field and/or dark-field illumination; and range-imaging methods, e.g. light sectioning.

For many metallic-surface inspection applications, neither bright- nor dark-field lighting, nor diffuse illumination, produce an acceptable image intensity. In fact, this is generally the case if the surface reflection properties change strongly across the intact surface: defects cannot be emphasized with regard to their background, and traditional intensity imaging techniques yield inferior performance. Surface defects with three dimensional characteristics—e.g. cavities, scratches, and nicks—are visualized with a larger contrast by means of range imaging. Since range imaging explicitly depicts surface height information, the data is less influenced by a change in the reflection factor across the surface.

In particular, our work¹ focuses on the inspection of rolled steel blocks that are partially covered with scale. Due to the strongly varying reflectance factor of the surface, traditional intensity imaging methods fail or have poor performance. As a result, range imaging based on fast light-sectioning techniques is used to acquire the three-dimensional shape of the steel block with its embedded flaws.

The light-sectioning method is a well-known measurement technique for optical determination of object sections. A light plane is projected onto the object from one direction, generally with a laser used as the light source. The profile that emerges of the scene is viewed from a different direction using a camera. Due to the known arrangement of the laser light source and the camera, the height information of the object can be determined in each point along the profile. The 3D model is gathered by moving the object in one direction while its cross-section is scanned in a sequential manner. Figure 1 shows a small nick in the edge of a steel block.

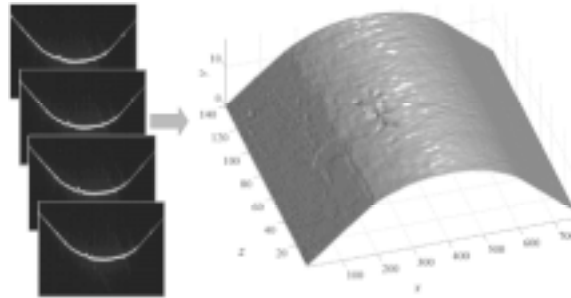


Figure 1. Acquired surface data of the nicked steel block.

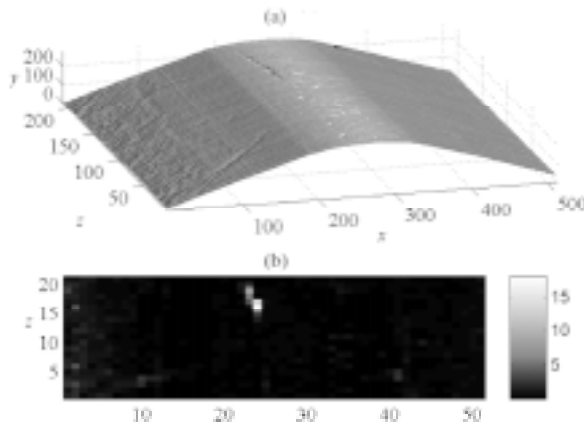


Figure 2. Analysis of the acquired data line by line: (a) Surface segment with crack. (b) Statistical measures computed for blocks of the orthogonal distance.

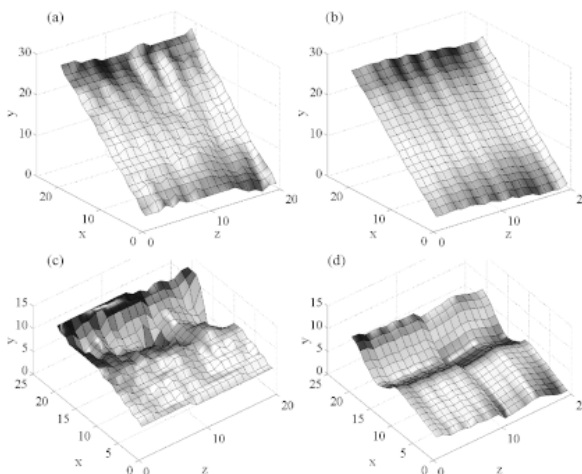


Figure 3. Surface approximation: (a) intact surface patch; (b) intact, smoothed surface approximant using the largest singular value; (c) flawed surface segment; (d) flawed smoothed surface approximant using the largest singular value.

Once the surface data have been acquired, they need to be analyzed for significant local deviations. Unfortunately, vibrations—caused by the movement of the steel block on the conveyor—result in the position of the profile varying in the range of a few millimeters. To compensate, a geometric transformation is applied to the different profile locations. The necessity for this transformation depends on the flaw detection approach taken. The transformation can be neglected if the defect-detection algorithm analyzes the data line by line. However, this spatial transformation is inevitable for a method based on segments of the surface area.

Basically, two different methods were considered for detecting the flaws. The first algorithm is based on a line-wise examination of the acquired profiles concerning significant geometric deformations. First, the acquired profile is approximated with a cubic spline to form a model. Second, the acquired profile is unwrapped by determining the distance from the data points orthogonal to the spline model. Finally, statistical measures of the orthogonal distance are computed for square blocks with a size of 10 pixels (see Figure 2).

The second method works with segments of the acquired surface data and is based on the mean square error of the orthogonal distance between the surface segment and its approximation. The surface approximant is gained by using singular value decomposition. It has been observed that the shapes of the intact surface segments are either planar or curved in one direction. Therefore, the first, largest singular value captures most of the variance of such simple surface shapes. In the case of a perturbation of the surface data caused by a flaw, a large amount of the surface shape is modelled by further additional singular values. Therefore, the idea is to assemble a smooth surface approximant by dropping all singular values except the first one (see Figure 3). Afterwards, the mean square error of the orthogonal distance between the segment and its approximant is determined and serves as local feature for flaw detection.

Our work shows reliable approaches for detection of small geometric defects on scale-covered steel surfaces by means of fast light sectioning.

Continues on page 10.

Automatic digital restoration of faded color films

Continued from cover.

more saturated colors than the rest of the image. This is because these zones are far from the mean (located at the origin of the principal axes). With respect to faded images, these zones correspond to areas that were saturated colors prior to fading. Thus, the scaling up brings out the colors of these zones. Moreover, considering the channel L^* in addition to a^* and b^* also permits the enhancement of image contrast: usually poor in faded images.

The next step is to balance the colors of the image. The color cast caused by the fading of the chromatic layers of the film, is non-uniform: i.e. it may have different colors and magnitude in shadows and highlights. This non-uniformity may be reinforced by the saturation-enhancement process. Classic color-constancy methods such as grey-world (GW) and white-patch (WP) may be simple and have low computational complexity, but they do not remove such non-uniform color casts caused by fading.

To fix this, the cast of the faded image has to be estimated within each of the image's different tones. The cast in highlights is better estimated by the white patch method, while the cast in mid-tones and shadows is better estimated by the grey-world method. The combination of these methods allows cast estimation and, so, correction in all the tones of the image. Our approach consists in correcting shadows with GW, and highlights with WP, but to avoid artifacts caused by loss of gradation in intensity levels, mid-tones are corrected with a graduated combination of the two methods. This hybrid method was tested on different images from different movies with different color casts and gave good results (see Figure 1(b)).

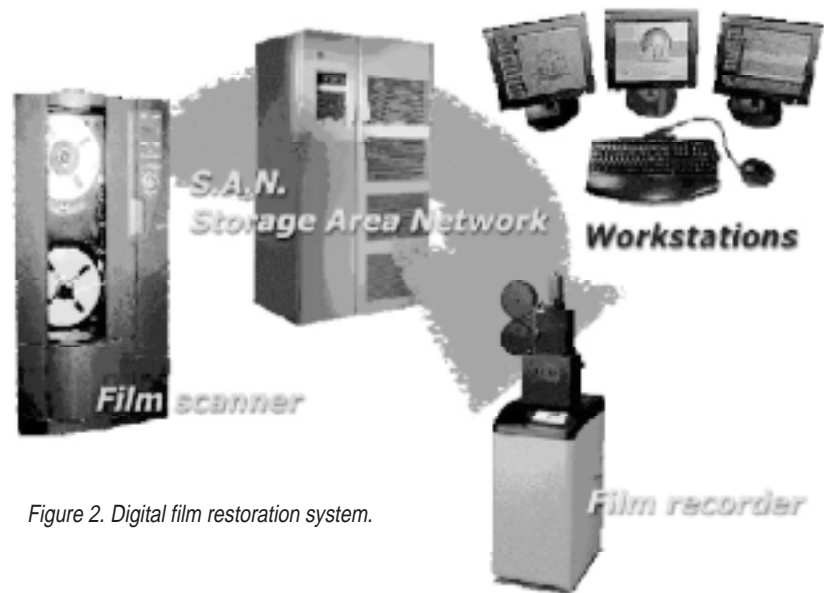


Figure 2. Digital film restoration system.

The user is able to make fine adjustments to the proposed correction prior to processing the whole sequence. One possible future enhancement of the system would be to integrate a learning facility to take into account user modifications and preferences, thus eventually minimizing the work required in this final step.

Majed Chambah

Eng., Ph.D.L31
Universite de La Rochelle
Avenue Michel Crepeau 1
7042 La Rochelle Cedex, France
E-mail: mchambah@univ-lr.fr

References

1. M. Chambah and B. Besserer, *Digital restoration of faded color movies: a four-step method*, **IS&T/SID 8th Color imaging conference CIC8**, pp. 161-166, Scottsdale, AZ, November 2000. <http://perso.univ-lr.fr/mchambah/docs/cic.pdf>.
2. M. Chambah, B. Besserer, and P. Courtellemont, *Recent progress in automatic digital restoration of color motion pictures*, **Proc. SPIE 4663**, pp. 98-109, San Jose, CA, USA, January 2002. <http://perso.univ-lr.fr/mchambah/docs/spie.pdf>.

Shape representation for color image querying

Continued from page 6.

values, a threshold of 28.9 is set to decide whether or not the rotated or shifted keys are the same as the original.

Figure 3 illustrates a set of more complex grayscale images, which contain 24bit colors with a single object on a white background. By visual inspection of Figure 3, we expect to find four groups of two shape classes viz., chairs, silverware, coffee cups, and clocks. The similarity results obtained for this setup are presented in Table 1. The results are close to those expected and deviations could be attributed to the effect of shift and rotation processes being performed in the digital domain, inaccurate rotation through small angles, and the lack of uniform KLD metrics. We are investigating the source of these deviations further. Our choice of KLD measures is also being reconsidered for application to images with multiple objects and complex backgrounds.

Mehmet Celenk, Qiang Zhou, Rakesh Godavari, and Vermund Vetnes

School of Electrical Engineering and Computer Science
Stocker Center, Ohio University
Athens, OH 45701, USA
Tel: 740/593-1581
Fax: 740/593-0007
E-mail: celenk@bobcat.ent.ohiou.edu

References

1. M. Celenk and S. Bobik, *Edge-suppressed color image indexing and retrieval*, **Proc. of CGIP (Int'l Conf. on Color in Graphics and Image Proc.)**, pp. 250-255, October 1-4, Saint-Etienne, France, 2000.
2. Y. Shao, *Higher Order Spectra Invariants for Shape Pattern Recognition*, **Ph.D. Dissertation**, Ohio University, 2000.
3. M. J. Swain and D. H. Ballard, *Color indexing*, **Int'l J. Computer Vision** 7 (1), pp. 11-32, 1991.

4. B. M. Mehre, et al., *Color matching for image retrieval*, **Pattern Recog. Lett.** 16, pp. 325-331, 1995.
5. Y. Rui, et al., *Image retrieval: Current techniques, promising directions and open issues*, **J. Visual Comm. & Image Repr.** 10, pp. 1-23, 1999.
6. A. K. Jain and A. Vailaya, *Image retrieval using color and shape*, **Pattern Recognition** 29 (8), pp. 1233-1244, 1996.
7. J. S. Lim, **Two-Dimensional Signal and Image Processing**, Prentice Hall, Englewood Cliff, NJ, 1990.
8. Y. Shao and M. Celenk, *Higher-order spectra (HOS) invariants for shape recognition*, **Pattern Recognition** 34, pp. 2097-2113, 2001.
9. R. M. Haralick and L. G. Shapiro, **Computer and Robot Vision Volume-I**, Addison-Wesley, Reading, MA, 1992.
10. R. C. Gonzalez and R. E. Woods, **Digital Image Processing**, Addison-Wesley, Reading, MA, 1992.
11. A. K. Jain, **Fundamentals of Digital Image Processing**, Prentice Hall, Englewood Cliff, NJ, 1989.

Electronic imaging for the inspection of wooden planks

Continued from page 5.

1s.

Real-time processing requires fast and accurate classification. Although a general best choice for a classifier does not exist, it should be selected according to the requirements and the nature of the classification problem. In our case, the classification is performed using the mixed fuzzy-logic approach and rule-based technique. This type of classification corresponds more closely to human classification, is fast, and has a simple hardware realization. The limiting factors, described earlier, produced unsatisfactory results using a neural-network based classifier.

Experimentally-obtained membership functions could, for example, look like the ones shown in Figure 4. They illustrate the length of the defect (H), the width of the defect (W), and the transverse position of the defect X_c inside the plank. The rules, for example, for one biological and one mechanical defect can be described as:

1. If the blob's location is in the *center* of the plank and its length is *medium* and its width is *medium* *knor*;

2. If V_1 is much less than V_2 and V_2 is equal to V_3 , then the profile has a *left wane*.

Radovan D. Stojanovic and George D. Papadopoulos
Industrial System Institute (ISI)
University Campus Rion
Patras, Greece
E-mail: radovan@isi.gr
<http://www.isi.gr>

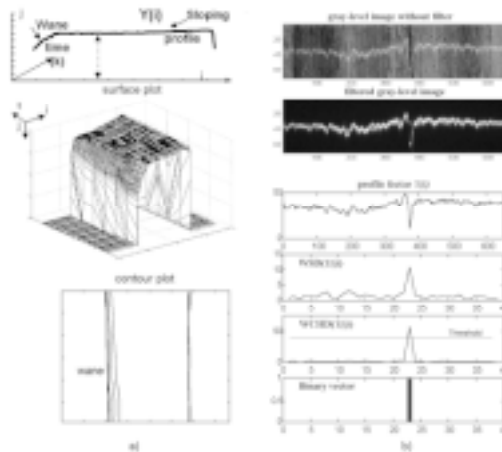


Figure 3. Detection of mechanical defects: (a) extracting shape and information and (b) finding cracks and splits.

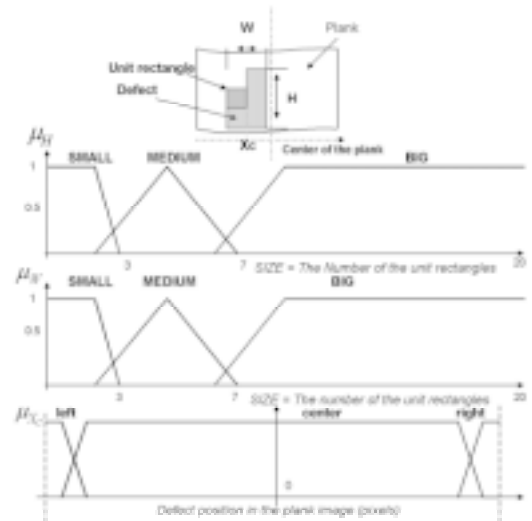


Figure 4. Fuzzy-logic grading (classification).

References

1. R. Stojanovic, G. Papadopoulos, P. Mitropulos, and I. Konstantinidis, *Robust System for Automated Wood Inspection*, **Proc. SPIE 4301**, pp.20-30, 2001.
2. R. Stojanovic, G. Papadopoulos, P. Mitropulos, M. Geogoudakis, R. Alcock, and I. Djurovic, *An Approach for Automated Inspection of Wood Boards*, **IEEE-ICIP MP.07.03**, 2001.

New Title from SPIE PRESS!

Adaptive Image Processing: A Computational Intelligence Perspective

By Stuart William Perry, Hau-San Wong, Ling Guan

Copublished with CRC Press

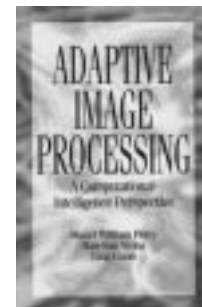
Application of computational intelligence techniques—often called soft computing—to the problem of adaptive image processing is the focus of this text. Imaging professionals and others with a background in mathematical science, computer software, and related fields will find this book a readable, useful resource.

SPIE PRESS Vol. PM116 • December 2001

282 pages • Hardcover 0-8194-4496-0

List price \$100; SPIE Members \$78

Order online today: www.spie.org/bookstore/



Eyetracking tools used to study photographers as they capture and edit digital photographs

Continued from page 12.

teers choose to crop a large fraction of their photographs when given the opportunity. An unexpected result was the type of crop decision made by observers. While observers often cropped 'person' photographs, they typically chose to enlarge the field for sculpture and interior scenes.

Along with the eyetracking results, this suggests that future systems might benefit from intelligent algorithms that suggest compositions for images captured in digital cameras. Increasing the number of photographs chosen for printing could have a significant impact on the profitability of digital photography.

This work was supported in part by a grant from the New York State Science, Technology,

and Academic Research program, and by Eastman Kodak.

Jason Babcock, Marianne Lipps, and Jeff B. Pelz

Carlson Center for Imaging Science
Rochester Institute of Technology
54 Lomb Memorial Drive
Rochester, NY 14623
E-mail: pelz@cis.rit.edu
<http://www.cis.rit.edu/pelz>

Automatic surface inspection of raw milled-steel blocks

Continued from page 7.

Franz Pernkopf,^a Friedrich Pernkopf,^b and Paul O'Leary^a

^aInstitute of Automation
Christian-Doppler Laboratory for Sensory Measurement

University of Leoben
8700 Leoben, Austria

E-mail: franz.pernkopf@unileoben.ac.at

^bDepartment of Engineering Mathematics
Geometry and Computer Science
University of Innsbruck
6020 Innsbruck, Austria

References

1. Franz Pernkopf, Friedrich Pernkopf, and Paul O'Leary, *Detection of surface defects on raw milled steel blocks using range imaging*, **Proc. SPIE 4664**, pp. 170-181, January 2002.

CALENDAR

2002

International Symposium on Optical Science and Technology

SPIE's 47th Annual Meeting

7-11 July

Seattle, WA USA

Call for Papers • Exhibition

<http://spie.org/conferences/calls/02/am/>

25th International Congress on High Speed Photography and Photonics

29 September-3 October

Beaune, France

SPIE will publish Proceedings

Call for Papers

<http://www-le2i.u-bourgogne.fr/hssp2002/>

Asian Symposium on Biomedical Optics and Photomedicine

21-23 October

Sapporo, Japan

SPIE is a cooperating organization

Program

<http://imd-www.es.hokudai.ac.jp/bopm2002/>



2nd International Conference on Imaging and Graphics

16-18 August

Hefei, China

SPIE will publish the Proceedings



International Symposium on Advanced Display Technologies

8-12 September

Crimia, Ukraine

Sponsored by SPIE Ukraine Chapter

2003

Electronic Imaging 2003

20-24 January

Santa Clara, CA USA

Call for Papers. Abstracts Due 24 June 2002

Exhibition

<http://electronicimaging.org/call/o3>



Photonics West

25-31 January

San Jose, California USA

Call for Papers. Abstracts Due 1 July 2002

Exhibition

<http://spie.org/conferences/calls/03/pw/>



For More Information Contact

SPIE • PO Box 10, Bellingham, WA 98227-0010

Tel: +1 360 676 3290 • Fax: +1 360 647 1445 • E-mail: spie@spie.org

Web: www.spie.org

Tell us about your news, ideas, and events!

If you're interested in sending in an article for the newsletter, have ideas for future issues, or would like to publicize an event that is coming up, we'd like to hear from you. Contact our technical editor, Sunny Bains (sunny@spie.org) to let her know what you have in mind and she'll work with you to get something ready for publication.

Deadline for the next edition, 13.1, is:

27 September 2002: Suggestions for special issues and guest editors.

14 October 2002: Ideas for articles you'd like to write (or read).

13 December 2002: Calendar items for the twelve months starting January 2003.

Join the SPIE/IS&T Technical Group

...and receive this newsletter

This newsletter is produced twice yearly and is available only as a benefit of membership in the SPIE/IS&T Electronic Imaging Technical Group.

IS&T—The Society for Imaging Science and Technology has joined with SPIE to form a technical group structure that provides a worldwide communication network and is advantageous to the memberships.

Join the Electronic Imaging Technical Group for US\$30. Technical Group members receive these benefits:

- *Electronic Imaging* Newsletter
- SPIE's monthly publication, *oe magazine*
- annual list of Electronic Imaging Technical Group members
- discounts on registration fees for IS&T and SPIE meetings and on books and other selected publications related to electronic imaging.

People who are already members of IS&T or SPIE are invited to join the Electronic Imaging Technical Group for the reduced member fee of US\$15.

Please Print Prof. Dr. Mr. Miss Mrs. Ms.

First (Given) Name _____ Middle Initial _____

Last (Family) Name _____

Position _____

Business Affiliation _____

Dept./Bldg./Mail Stop/etc. _____

Street Address or P.O. Box _____

City _____ State or Province _____

Zip or Postal Code _____ Country _____

Phone _____ Fax _____

E-mail _____

Technical Group Membership fee is \$30/year, or \$15/year for full SPIE and IS&T Members.

Amount enclosed for Technical Group membership \$ _____

I also want to subscribe to IS&T/SPIE's *Journal of Electronic Imaging* (JEI) \$ _____
(see prices below)

Total \$ _____

Check enclosed. Payment in U.S. dollars (by draft on a U.S. bank, or international money order) is required. Do not send currency. Transfers from banks must include a copy of the transfer order.

Charge to my: VISA MasterCard American Express Diners Club Discover

Account # _____ Expiration date _____

Signature _____
(required for credit card orders)

Reference Code: 3152

JEI 2002 subscription rates (4 issues):

	U.S.	Non-U.S.
Individual SPIE or IS&T member	\$ 55	\$ 55
Individual nonmember and institutions	\$245	\$265

Your subscription begins with the first issue of the year. Subscriptions are entered on a calendar-year basis. Orders received after 1 September 2002 will begin January 2003 unless a 2002 subscription is specified.

Send this form (or photocopy) to:
SPIE • P.O. Box 10
Bellingham, WA 98227-0010 USA
Tel: +1 360 676 3290
Fax: +1 360 647 1445
E-mail: membership@spie.org

Please send me:

- Information about full SPIE membership
- Information about full IS&T membership
- Information about other SPIE technical groups
- FREE technical publications catalog

Electronic Imaging

The *Electronic Imaging* newsletter is published by SPIE—The International Society for Optical Engineering and IS&T—The Society for Imaging Science and Technology. The newsletter is the official publication of the International Technical Group on Electronic Imaging.

Editor/Technical Group Chair Arthur Weeks
Technical Editor Sunny Bains
Managing Editor/Graphics Linda DeLano
Advertising Sales Gayle Lemieux

Articles in this newsletter do not necessarily constitute endorsement or the opinions of the editors, SPIE, or IS&T. Advertising and copy are subject to acceptance by the editors.

SPIE is an international technical society dedicated to advancing engineering, scientific, and commercial applications of optical, photonic, imaging, electronic, and optoelectronic technologies.

IS&T is an international nonprofit society whose goal is to keep members aware of the latest scientific and technological developments in the fields of imaging through conferences, journals and other publications.

SPIE—The International Society for Optical Engineering, P.O. Box 10, Bellingham, WA 98227-0010 USA. Tel: +1 360 676 3290. Fax: +1 360 647 1445. E-mail: spie@spie.org.

IS&T—The Society for Imaging Science and Technology, 7003 Kilworth Lane, Springfield, VA 22151 USA. Tel: +1 703 642 9090. Fax: +1 703 642 9094.

© 2002 SPIE. All rights reserved.

EIONLINE

Electronic Imaging Web Discussion Forum

You are invited to participate in SPIE's online discussion forum on Electronic Imaging. The **INFO-EI** mailing list has been 'retired' as we move the discussions to the more full-featured web forums. We hope you will participate. To post a message, log in to create a user account. For options see "subscribe to this forum."

You'll find our forums well-designed and easy to use, with many helpful features such as automated email notifications, easy-to-follow 'threads,' and searchability. There is a full FAQ for more details on how to use the forums.

Main link to the new Electronic Imaging forum:

<http://spie.org/app/forums/tech/>

Related questions or suggestions can be sent to forums@spie.org.

Eyetracking tools used to study photographers as they capture and edit digital photographs

Digital photography is changing the photographic marketplace. Once a digital camera is purchased, profits are tied to consumers' decisions to print individual photographs, so understanding how consumers judge their own images is crucial. Many elements contribute to perceived quality, but amateurs often report dissatisfaction with images based on the composition of photographs they themselves composed.

While one might predict strong similarities between composing a scene and viewing the resultant photograph, it appears that consumers treat the two cases very differently, using different strategies and applying distinctly different criteria. One hypothesis is that consumers focus their attention only on the primary object during image capture, but pay attention to broader regions while judging images. To study consumer behavior before and after image capture, we have developed instrumentation to monitor the eye movements of photographers as they explore and photograph scenes.

The human retina is highly anisotropic; the effective density of photoreceptors falls by an order of magnitude just degrees from the central fovea. The resultant variation in spatial resolution requires that the eyes be moved to view objects with even moderate detail. In addition to eye movements forced by acuity limits, the eyes are also directed to areas of attention. Thus observers' attention can be monitored by measuring their eye movements. It has been shown that self-report is not a reliable method for determining attention during a task, as the deployment of attention is typically accomplished below the level of conscious awareness.

Figure 1 shows the self-contained wearable eyetracker. Current experiments at the Carlson Center for Imaging Science at the Rochester Institute of Technology are using the unique sys-



Figure 1. Left: RIT wearable eyetracker. Right: Video eyetracker record. The black crosshair indicates the observer's point of gaze in the scene.

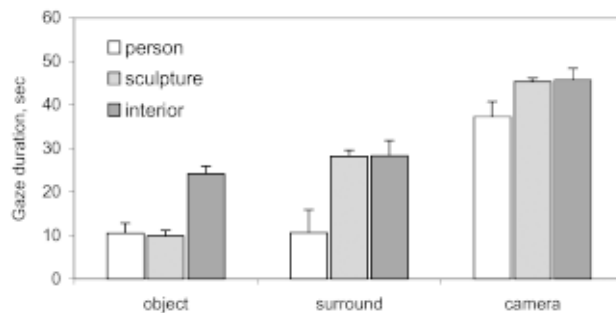


Figure 2. Gaze duration during image-capture for the 'person,' 'sculpture,' and 'interior' scenes. Total time was parsed by the photographers' point of regard.



Figure 3. Left: observer wearing head-mounted eyetracker. Right: The black crosshair indicates the observer's point of gaze.

tem to better understand the behavior of amateur photographers. Observers performed two tasks. In the *image-capture* task they took nine digital photographs of a person, a large sculpture, and an interior architectural scene. In the *image-edit* task they selected and cropped three

of those photographs. Their eye movements were monitored during both tasks.

For analysis in the image-capture task, each visual fixation was identified as being focused on the primary object of the photograph (*object*), the regions surrounding the primary object (*surround*), or on the digital camera's controls and LCD display (*camera*). Figure 2 shows the highly scene-specific viewing behavior; while observers spent the same amount of time looking at the camera regardless of the scene, the time spent looking at the primary object or surround differed significantly depending on which scene was being photographed.

Figure 3 shows an observer performing the image-edit task. Analysis showed that observers fixated semantic-rich regions in each image, though the spread of fixations, edit time, and number of crop windows did not differ significantly across the person, sculpture, and interior classes. This suggests that the image-edit task was less influenced by image content.

The experimental design also included a study of consumers' choices in cropping the images. With current cameras, consumers can crop individual photographs by excluding some of the original image. The digital camera's preview LCD was masked so the camera captured a larger portion of the scene than was evident to the photographer. This modification allowed the observers three options during the image edit task; leave the image as captured, crop the image, or extend a photograph's borders beyond the original.

During image capture 75% of the observers used the camera's zoom feature. When given the option to crop the image during the image-edit task, 90% of the observers chose to crop the images, confirming reports that ama-

Continues on page 10.